6-9-2020

Effect of Electrode Placement on Defibrillation Threshold and Esophageal Electric Field in Internal Atrial Defibrillation

Andrew Arnold Bryant

EFFECT OF ELECTRODE PLACEMENT ON DEFIBRILLATION THRESHOLD AND ESOPHAGEAL ELECTRIC FIELD IN INTERNAL ATRIAL DEFIBRILLATION

by

Andrew Bryant

A Thesis

Submitted in Partial Fulfillment of the

Requirements for the Degree of

Master of Science

Major: Biomedical Engineering

The University of Memphis

May 2020

ACKNOWLEDGEMENTS

I want to thank Dr. Amy Curry for being my advisor and providing me guidance throughout the research process. Without her help, I would not have been able to complete this work. I also want to thank my committee members, Drs. John Williams and Judith Soberman, who provided great insight and advice into my research. Also, Dr. Madhu Balasubramanian greatly helped me with my COMSOL simulations, and I am grateful for that.

I would also like to thank my wife Leah and my family and friends for supporting me over these past years. Most of all, I give great thanks and all glory to my God and Savior, Jesus Christ, who has given me the strength and ability to complete this work.

ABSTRACT

Atrial fibrillation is the most common heart arrhythmia of clinical significance. Internal cardioversion can be used to restore normal sinus rhythm; however, the amount of delivered energy elicits intolerable pain. Lowering delivered energy could make implantable cardioverters a promising treatment option. This study simulated cardioversion shocks in a model of the human heart using finite element analysis to determine effects of different electrode placements on defibrillation threshold (DFT) and esophageal electric field (EEF) near the left atrium. Ten right atrial to coronary sinus electrode placements were tested. Small shifts in electrode placements changed DFT by up to 42%, indicating electrode position is an important factor in lowering DFT. A relationship was not discovered between EEF and DFT. If a relationship can be discovered between an alternate EEF or other measure and DFT, electrode placements could be optimized on a patient-specific basis to lower delivered energy to painless or tolerable levels.

TABLE OF CONTENTS

Contents	Page
List of Tables	v
List of Figures	vi
1. Introduction/Background	1
2. Objectives	4
3. Methods	5
Anatomical Model	5
Finite Element Simulations	11
Data Analysis	13
4. Results	14
Mesh Convergence Study	15
Electric Field Distribution	16
DFTs, Average EEFs, and Regression Analysis	19
5. Discussion	21
Effect of Electrode Placement on DFTs and Average EEFs	22
Model Limitations	23
Future Work	23
6. Conclusions	24
References	26

LIST OF TABLES

Table	Page
1. Number of Tetrahedra and Total Volume of the Heart Regions	7
2. Electrical Conductivity Values of Each Tissue Region	12
3. Number of Tetrahedra in Heart for Mesh Convergence	14
4. DFTs and Volumes of Atrial Myocardium in Mesh Convergence Study	15
5. DFT Voltages for Each Electrode Configuration	20

LIST OF FIGURES

Figure Page

1. Original threshold of cardiac anatomy in the axial view, where A indicates anterior, P indicates posterior, R indicates right, L indicates left, 60.00 indicates slice number, and -160.00 indicates table position, which is the location of the examination table as the CT scanning proceeds. 8

2. Anterior/posterior view of the epicardial surfaces of the right and left atrium and right and left ventricles. 8

3. Isometric view of the model. The myocardium is shown in pink (ventricular) and grey (atrial), lungs in green, esophagus in yellow and descending aorta in purple. 9

4. Axial view of contours of the volume mesh of the atrial and ventricular myocardium. Atrial myocardium in pink, ventricular myocardium in white. Inset shows a portion of interface between atria and ventricles. 9

5. Lateral views of: a. atrial myocardium with coronary sinus displayed. b. atrial myocardium with CS1 electrode. c. atrial myocardium with CS2 electrode. d. right atrium with right atrial electrodes notated from left to right as: RAL1, RAL4, RAL2, RAL3, and RAS5. CS = Coronary Sinus, RAL = Right Atrial Lateral, RAS = Right Atrial Septal. Epicardial and endocardial surfaces are transparent. 10

6. Lateral view of atrial myocardium and esophagus, indicating the approximate range of electric field data extracted from the esophagus. 13

7. Anterolateral views of electric field in atrial myocardium of CS2_RAL1: a. coarse mesh; b. fine mesh; c. finer mesh, and posterolateral views of electric field in atrial myocardium of CS2_RAL1: d. coarse mesh; e. fine mesh; f. finer mesh of the mesh convergence study. 15

8. Electric field distribution in the atrial myocardium for CS1_RAL4 configuration in the atrial myocardium. Electric field values are in V/cm. 16

9. Electric field distribution in the atrial myocardium for CS2_RAL4 configuration in the atrial myocardium. Electric field values are in V/cm. 17

10. Electric field distribution in the atrial myocardium for CS1_RAS5 configuration in the atrial myocardium. Electric field values are in V/cm. 17

11. electric field distribution in the atrial myocardium for CS2_RAS5 configuration in the atrial myocardium. Electric field values are in V/cm. 18

12. Lateral views of electric field distribution in the atrial myocardium and esophagus for four different electrode configurations: a. CS1_RAL3; b. CS2_RAL3; c. CS1_RAL4; d. CS2_RAL4; electric field values are in V/cm. 19

13. Average EEF with standard deviation bars for each electrode configuration. 20

14. The comparison between the normalized dfts and normalized average eefs for each electrode configuration. The coefficient of determination shows there is no relationship between the DFTs and average EEFs for these given electrode configurations. 21

Introduction/Background

Atrial fibrillation (AF) is the most common heart arrhythmia throughout the U.S. and European countries and is the most clinically significant arrhythmia, affecting over 33 million people worldwide.[1] As the population grows older, AF is becoming more prevalent in older patients. Patients in the age range of 65-85 years old make up approximately 70% of AF cases.[2] Several studies have reported AF incidence and prevalence, and the majority predict that the prevalence of AF will increase rather rapidly in the coming years.[3-5] In the U.S., some studies predict that the number of people having AF in the year 2050 will be 5.6 million[6], while another study predicts that number to be as high as 12 million.[5] In Europe, that number is predicted to be even higher at 17 million in the year 2060.[5] With the increasing number of cases of AF, the U.S. national healthcare costs to treat this arrythmia range from $6 billion up to $26 billion and include inpatient, outpatient and pharmacy costs.[7] This growing concern calls for more effective treatments to prolong the quality of life for people affected by AF.

AF is a supraventricular tachycardia (SVT) in which there are rapid, irregular contractions of the muscle fibers in the atria. These irregular contractions are often due to reentrant electrical wavefronts and are associated with a variety of health risks for those with AF, including stroke, valvular heart disease, hypertension and other potential life-threatening conditions if not properly treated.[8]

AF has been treated over the years by a range of methods in order to return the heart to sinus rhythm, including electrical cardioversion, antiarrhythmic drug therapies and ablation. The efficacy of each method is dependent upon each patient, namely the severity of AF, other health (especially cardiac) related problems and the length of time experiencing AF. Some of the antiarrhythmic drugs prescribed for treatment of AF include dofetilide, flecainide, propafenone,

sotalol and quinidine. These drugs aim to alleviate reentrant wavefronts, but do not have constant efficacy.[9] When these drugs do not effectively treat a patient, catheter ablation can be performed to prevent the recurrence of AF by first sedating the patient, inserting one or more intravenous catheters with electrodes, recording and pacing in various intracardiac locations, followed by directed radiofrequency (RF) energy to burn and destroy the tissue causing the reentrant electrical wavefronts.[10] However, this is an invasive surgical procedure and even when successful, ablation is often needed more than once. External cardioversion is a common technique performed clinically, typically using self-adhesive electrodes applied to the anterior and/or posterior chest. A shock or series of shocks is delivered to the patient's chest to restore sinus rhythm. Similarly, internal cardioversion is a viable means to successfully restore sinus rhythm, with catheter electrodes inserted intravenously inside the patient's heart. Animal and human studies have verified the efficacy of internal cardioversion for AF[11-12] and implantable cardioversion devices could be an effective treatment alternative. However, the major limiting factor for internal cardioversion of AF via an implantable device is that the amount of energy currently required to restore sinus rhythm elicits pain and discomfort to the patient. Several studies have shown that low energy shocks greater than 2 J can cause intolerable pain to patients.[13-15] One study explored different mechanisms of pain as a result of internal defibrillation shocks that ranged from 50-500 V.[16] The human pain threshold of approximately 1-2 J makes internal defibrillation a limited, sometimes impossible solution for treatment of AF.[17]

There have been numerous animal, human and simulation studies to develop and test techniques to lower the amount of delivered energy to the patient with an implantable defibrillator in order to reduce delivered energy to near or below the human pain threshold and still successfully terminate AF. Different strategies to determine if the delivered energy can be

lowered to the desirable range have been studied. Waveform optimization has been explored to determine which type of waveform, such as monophasic or biphasic waveform, is most effective for internal cardioversion. One study tested a passive implantable atrial defibrillator (having no battery or discharging capacitor and driven solely by RF energy) that delivered a low-tilt monophasic waveform, compared to three different biphasic waveforms, to determine if waveform selection can improve the efficacy of defibrillation.[18] Another strategy to lower the delivered energy is to predict an optimal electrode placement. Various human and animal studies have tested several different electrode configurations, including a right atrium to coronary sinus configuration, defibrillator "can" to right ventricle and right atrium configuration and right atrium to left pulmonary artery configuration, and have compared the rates of atrial defibrillation success for each configuration. The right atrial-coronary sinus configuration has been found to successfully defibrillate the heart with the least amount of energy, and as a result this is a common clinical electrode configuration. One study showed that this configuration greatly lowered the DFT compared to a different configuration, with 91% of patients having restored sinus rhythm.[19] A separate simulation study tested three different electrode configurations in a canine heart to determine various factors after electric field exposure, including amount of atrial myocardium damaged, inter-electrode impedance, electric field strength and the magnitude of the voltage gradient. The electrode configurations tested indicated a lower impedance, stronger electric field strength in the atrial myocardium and minimal myocardial damage.[20] Another potential factor in determining an optimal electrode placement is the idea that esophageal electric fields (EEFs) can be predictive of atrial cardioversion success. Fitch et al. performed a finite element analysis in external cardioversion, testing over 600 electrode configurations, determining that small shifts in the electrode placement from an initial

clinically relevant position can lower the defibrillation threshold (DFT), defined as the applied voltage required to produce an electric field of 5 V/cm throughout the atrial myocardium.[21] In a separate study, Fitch et al. investigated the relationship between EEFs and DFTs by inducing and cardioverting AF in pigs. The results indicated a strong negative relationship between the EEFs and DFTs, indicating that EEFs could be a potential predictor for optimal electrode placements.[22] If an optimal electrode placement can be predicted using EEFs measured prior to cardioversion, the energy delivered to the patient could be lowered to tolerable pain levels.

Objectives

The purpose of this study was to determine the effects of various electrode placement(s) on the DFTs required for internal cardioversion of atrial fibrillation and explore a potentially predictive measure for lowering DFTs. This overall goal was achieved through the following objectives: (1) simulate cardioversion shocks in an anatomically realistic model of the heart using finite element analysis, (2) determine the effect of various electrode placements on delivered energy, and (3) determine if a positive or negative relationship exists between electric field in the esophagus and DFTs. First, an anatomically realistic model was developed by extracting 3D surfaces from stacked computed tomography (CT) images of the heart. The anatomy consisted of the heart with both atrial and ventricular myocardium and blood pools, the descending aorta, the lungs and the esophagus, surrounded by a bounding box to ensure proper boundary conditions. Electrode geometry was created and inserted into different locations in the right atrium and coronary sinus region. Finite element analysis was performed in COMSOL to determine the electric fields produced in the atrial myocardium by ten different electrode configurations. The atrial electric field data were exported and used to determine the DFT. Additionally, the average electric field strength produced in a selected region of the esophagus

was analyzed to determine whether it correlated with the DFT of the atrial tissue and thus aid in determining optimal electrode placement.

Methods

Anatomical Model

The software used to develop the anatomical geometry was Materialise MIMICS Research version 21.0 and Materialise 3-Matic Research version 13.0. The CT scan used was the heart_se.mcs file that is provided with the student edition of the MIMICS software. The CT images were taken from a 55-year old female in October 2007 using a LightSpeed VCT scanner from GE Medical Systems. The scan contains 193 slices with a slice thickness of 0.625 mm. Information from Materialise's HeartPrint® Imaging Guidelines[23] gives a general rule for cardiac scan protocol; that the images are obtained using a "standard ECG-triggered diastolic protocol with good contrast," and more notably that ideally the heartbeat is below 65 bpm and the patient is holding her breath. Also, to better understand the anatomy of the patient, an anatomical atlas was referenced to specify the locations of various parts of the heart and other organs.[24]

To begin developing the 3D models of each individual organ, the heart_se.mcs file was opened in MIMICS, and segmentation by thresholding of the CT image was performed to highlight the specific anatomy that needed to be modeled. The primary focus of the modeling process was the heart, and the accuracy of the four endocardial surfaces of the heart as well as the myocardial tissue were the most important aspect of the model. To easily extract the electric field data in the atrial myocardium, the myocardium was split between its atrial and ventricular components.

After performing an initial thresholding operation, implementation of the region growing tool aided in distinguishing between the different organs and creating separate masks for each individual organ. Next, a 3D part was created using the "high quality" parameter setting for each organ using an adapted marching cubes algorithm.[25] If the 3D model did not include all the surface needed, more segmentation was performed including multiple slice editing. Once the desired accuracy and level of detail for each anatomical component was achieved, each model was exported to 3-Matic. Working in 3-Matic, each model was refined further by using the *wrap* and *smooth* operations. Wrapping the models serves to close in holes, smooth out each 3D part, and remove internal shells, creating a sealed, watertight model. The *smooth* operation smooths the model and decreases the sharp edges throughout. Similarly, *local smoothing* allows for smoothing in certain areas of the geometry which need refining as opposed to the entire geometry. The myocardium was hollowed by performing a *Boolean subtraction* of the myocardium from the endocardial surfaces. To ensure the nodes of the tetrahedra in the myocardium aligned properly, a *non-manifold assembly* joined the atrial and ventricular myocardium, then subsequently the parts were separated, and the interface of the assembly was joined to both myocardial parts. Performing an *adaptive remesh* on the surface on each part with the skewness shape measure ensured a high-quality mesh. The final step before volume mesh creation was to utilize the *fix wizard* to check for any holes, overlapping and intersecting triangles and inverted normals. These steps were repeated until all errors were fixed and the desired mesh quality was achieved.

The electrode geometries were created in 3-Matic using the analytical primitives menu. Because studies have shown that the right atrial-coronary sinus electrode configuration can successfully defibrillate the heart with the lowest amount of delivered energy, this configuration

was chosen for investigation in this study. Two electrodes were created near the coronary sinus region and five electrodes were placed in the right atrium. Volume meshes were then created for each part of the model, including all organs, the bounding box and the electrodes. Before exporting the volume meshes to COMSOL, the final step was to view the contours of the volume meshes in MIMICS to verify that the mesh nodes matched up appropriately. Table 1 lists the number of tetrahedra in several meshes of the model as well the total volume of those meshes.

Table 1: Number of Tetrahedra and Total Volume of the Heart Regions

Anatomy	**Number of Tetrahedra**	**Total Volume (mm^3)**
Atrial Myocardium	243,060	138,500
Ventricular Myocardium	373,909	232,100
Atrial Blood Cavity	168,663	114,500
Ventricular Blood Cavity	242,677	167,100

The figures below indicate several stages of the modeling process, including the original threshold of the cardiac anatomy (Figure 1), anterior and posterior views of the 3D heart model (Figure 2), an isometric view of the entire model with all anatomy included (Figure 3), an axial view of the contours of the volume meshes of the atrial and ventricular myocardium (Figure 4) and a panel of all the electrode placements (Figure 5).

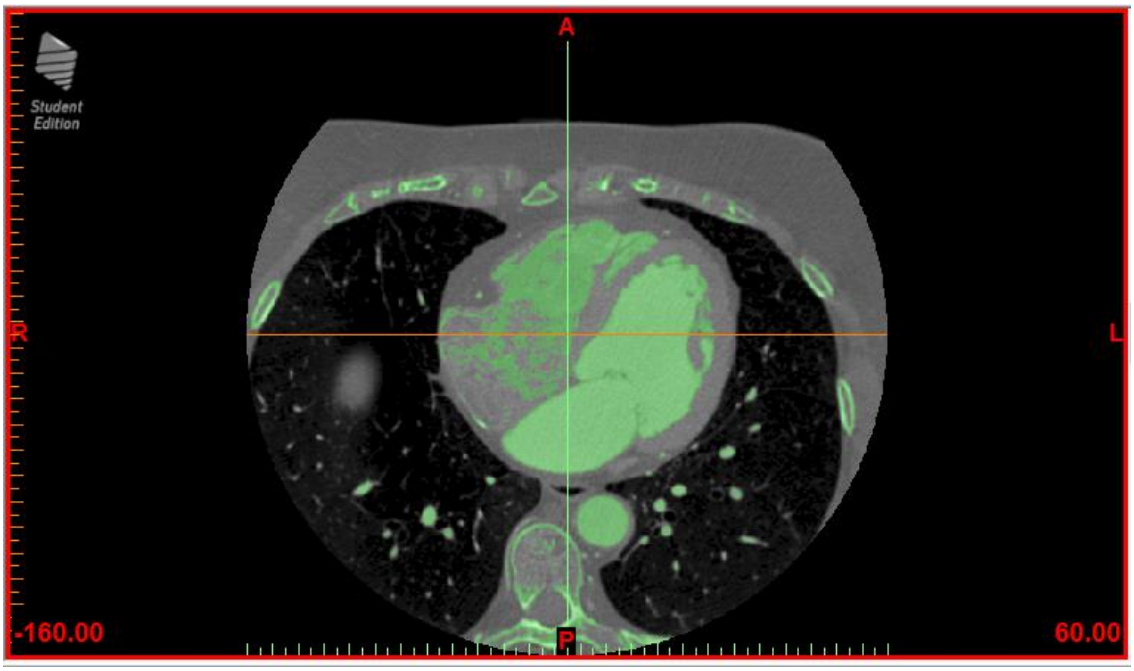

Figure 1: *Original threshold of cardiac anatomy in the axial view, where A indicates anterior, P indicates posterior, R indicates right, L indicates left, 60.00 indicates slice number, and -160.00 indicates table position, which is the location of the examination table as the CT scanning proceeds.*

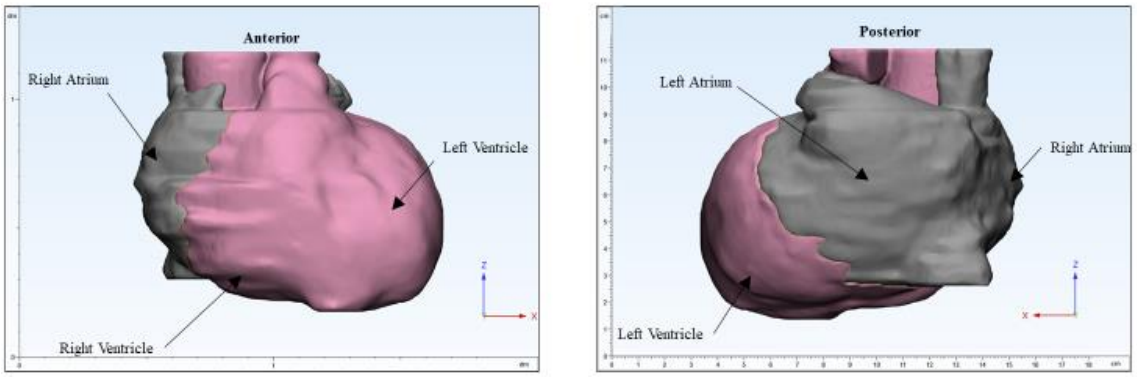

Figure 2: Anterior/posterior view of the epicardial surfaces of the right and left atrium and right and left ventricles.

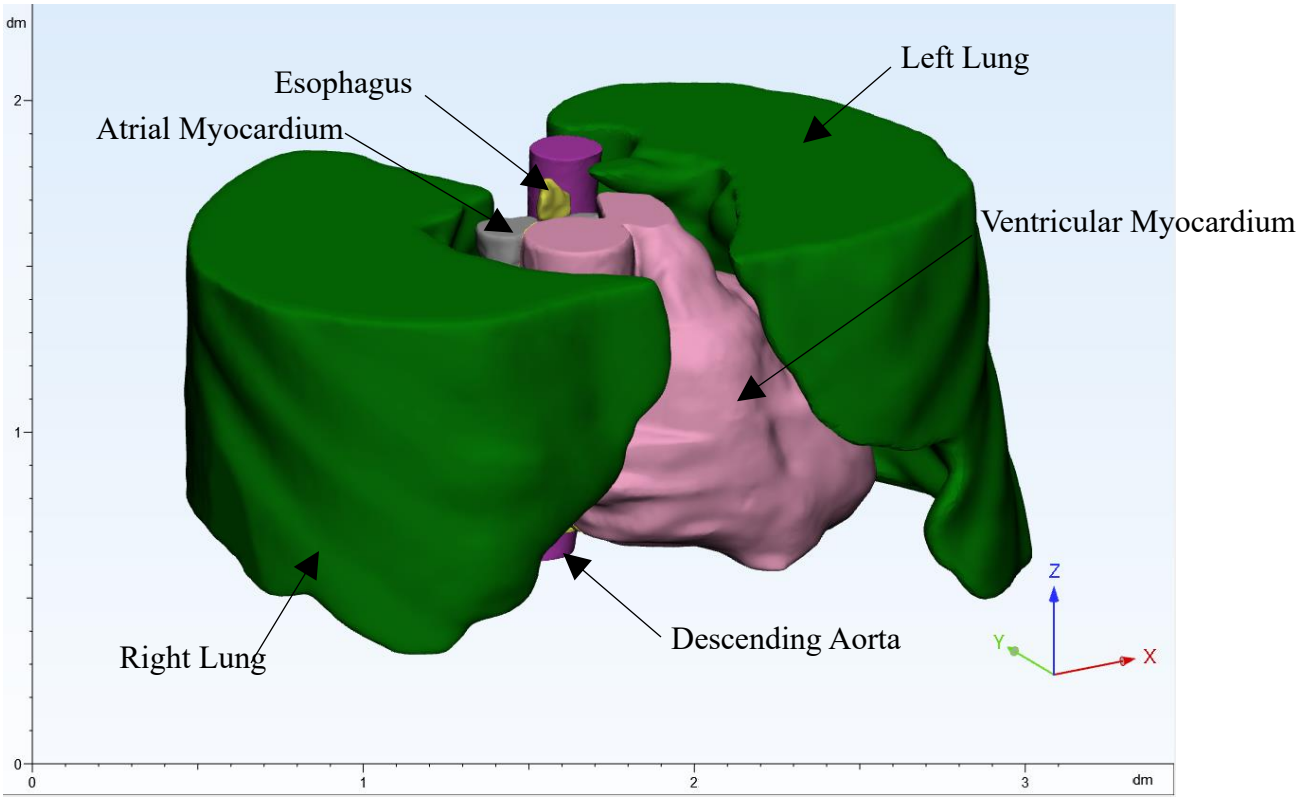

Figure 3: Isometric view of the model. The myocardium is shown in pink (ventricular) and grey (atrial), lungs in green, esophagus in yellow and descending aorta in purple.

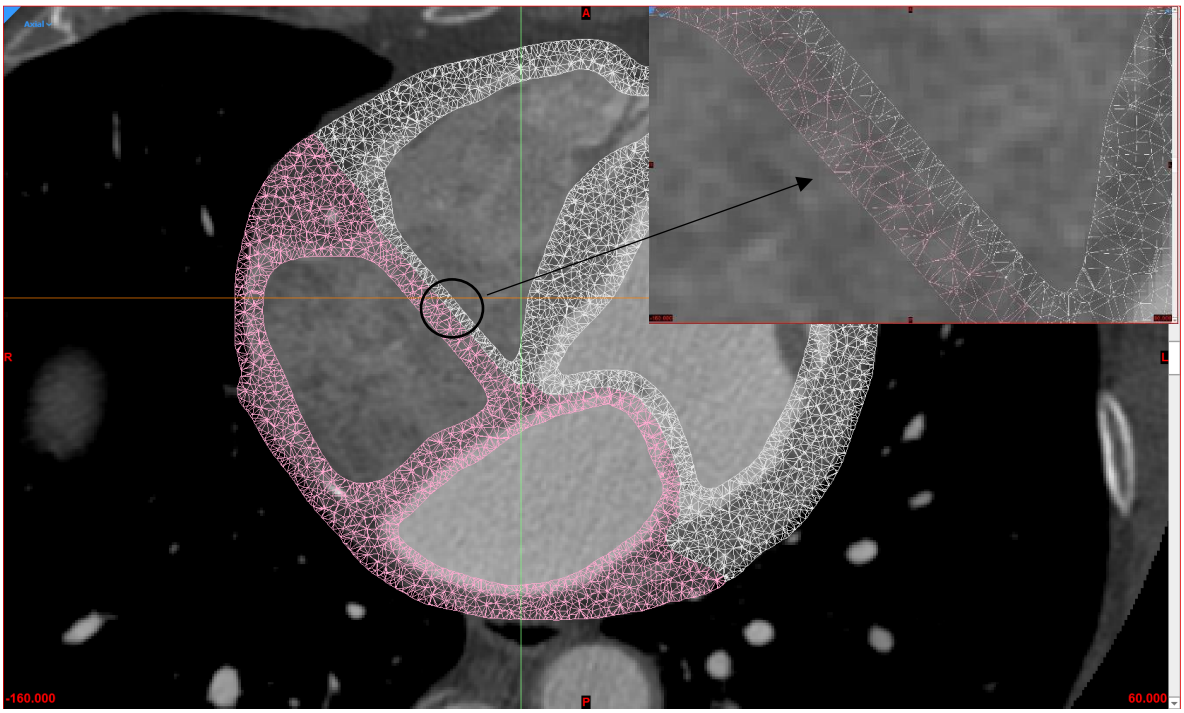

Figure 4: Axial view of contours of the volume mesh of the atrial and ventricular myocardium. Atrial myocardium in pink, ventricular myocardium in white. Inset shows a portion of interface between atria and ventricles.

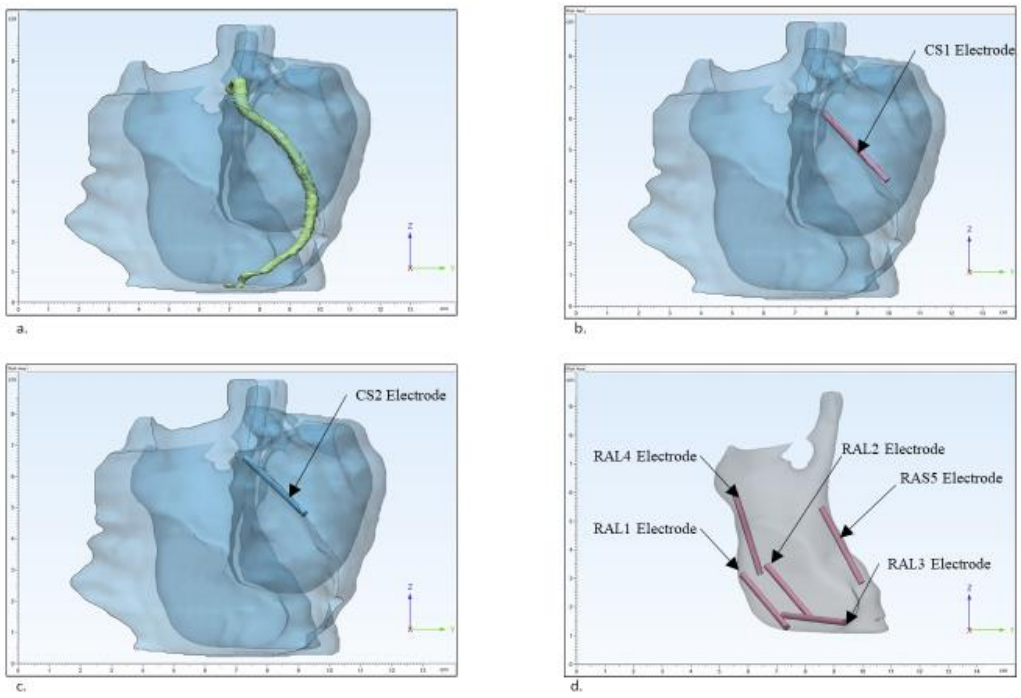

Figure 5: Lateral views of atrial electrode placements: a. atrial myocardium with coronary sinus displayed as an opaque surface, b. atrial myocardium with CS1 electrode, c. atrial myocardium with CS2 electrode, and d. right atrium with right atrial electrodes notated from left to right as: RAL1, RAL4, RAL2, RAL3, and RAS5. CS = Coronary Sinus, RAL = Right Atrial Lateral, RAS = Right Atrial Septal. Epicardial and endocardial surfaces are transparent.

For the purposes of this study, two electrodes were tested in each simulation, with the coronary sinus electrode (CS1) being stationary, and the right atrial electrode shifting to five different locations along the lateral and septal wall. The coronary sinus electrode was shifted to a new location (CS2), and the same five right atrial electrode locations were tested, for a total of ten electrode configurations. The notation of the electrode configurations is CS1_RAL1, CS1_RAL2, CS1_RAL3, CS1_RAL4, CS1_RAS5, CS2_RAL1, CS2_RAL2, CS2_RAL3, CS2_RAL4 and CS2_RAS5.

Finite Element Simulations

The simulations were carried out in COMSOL Multiphysics 5.4 through the Research Desktop of the Citrix Workspace virtual computing environment at University of Memphis. Simulated cardioversion shocks were tested in the anatomically realistic, volume conductor model of the heart using finite element meshes and finite element analysis. To begin work on the simulations, the meshes were imported into COMSOL. After importing each mesh, the boundaries of each mesh were explicitly defined to set up identity boundary pairs between the boundaries of two separate meshes that had touching boundaries. These identity boundary pairs ensure continuity on the interior boundaries of the touching meshes to allow current to flow properly through the entire model.

Once all the boundaries of the meshes were appropriately defined, the electric currents physics module was implemented to define electrical conductivity values of the various tissues and blood, continuity on the interior boundaries and the electric potential at the electrodes. The governing formulation is Laplace's equation:

$$\vec{\nabla}.\overline{\sigma}\nabla\phi = 0 \qquad (1)$$

where, $\overline{\sigma}$ represents the conductivity as a tensor and ϕ is the electric potential. The Neumann or natural boundary conditions are applied on the body surface, in which current can neither enter nor leave the volume except at the locations of the defibrillation electrodes. A stationary, non-time varying study with isotropic conductivities (scalar σ) was performed to determine the electric field distribution in the atria and esophagus. The bounding box as well as the esophagus were assigned the conductivity of connective tissues, and the endocardial surfaces were assigned the conductivity of blood. Table 2 lists these conductivity values, as reported by Rush and Geddes.[26-27]

Table 2: Electrical Conductivity Values of Each Tissue Region

Tissue Region	Conductivity (S/m)
Connective Tissue Esophagus	0.222
Ventricular Myocardium Atrial Myocardium Descending Aorta	0.25
Ventricular Blood Pool Atrial Blood Pool Descending Aorta Blood Pool	0.667
Lungs	0.078

The electric currents module in COMSOL was used for the finite element formulation. After assigning all conductivity values, continuity was defined on interior boundaries to ensure current flowed through all the tissue and electrical potential difference of 200 V was applied to the electrodes, then the study was computed. After completing a simulation, plots of the electric field in the atrial myocardium and esophagus were observed qualitatively, and the electric field values of the atrial myocardium and esophagus were extracted to a text file. The text files included the x, y and z coordinates of the center of each tetrahedron, the volume of each tetrahedron and the electric field value of each tetrahedron at those coordinates. The electric field data points were extracted from the centroid of each tetrahedron using the Gauss integration point. For the esophageal data, only the values in tetrahedra most adjacent to the left atrium between z-coordinates of -170 to -190 mm were exported, as shown in Figure 6 below. Each text file of data was then imported in Excel for data analysis.

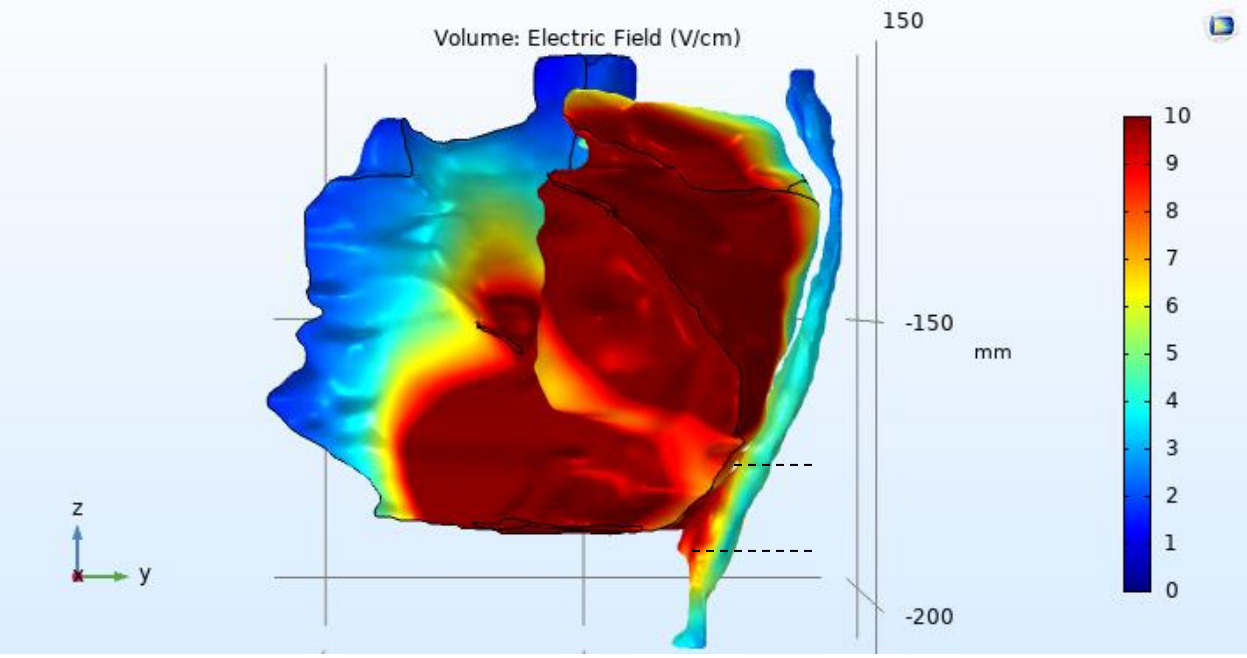

Figure 6: Lateral view of atrial myocardium and esophagus, with dashed lines indicating the approximate range of electric field data extracted from the esophagus.

Data Analysis

To determine the DFT voltage, the applied voltage to the electrodes was scaled to produce a minimum electric field of 5 V/cm in 95% of the tetrahedral volume elements representing the atrial tissue. The electric field values were sorted in ascending order, and the volumes of the corresponding tetrahedra were summed until 95% of the atrial volume was reached. To verify the simulations, the simulations were computed again, applying the DFT voltages rounded to the nearest whole number on the electrodes. The data was extracted again, and the volumes summed up to 95% of the atrial volume. The electric field at 95% of the volume yielded 5 V/cm, thus verifying the simulation. The average electric field in the portion of the esophagus adjacent to the atria was calculated.

A brief mesh convergence study was performed, testing the model with a coarser and finer mesh of the heart for the CS2_RAL1 electrode configuration to determine any changes in

the DFT. Table 3 below lists the number of tetrahedra and total volumes of the heart in each mesh. The fine mesh was implemented in all ten electrode configurations.

Table 3:Number of Tetrahedra in Heart for Mesh Convergence

Anatomical Part	Coarse Mesh Tetrahedra	Fine Mesh Tetrahedra	Finer Mesh Tetrahedra
Ventricular Myocardium	255,373	373,909	975,121
Atrial Myocardium	138,524	243,060	696,874
Ventricular Blood Pool	188,107	242,677	506,139
Atrial Blood Pool	145,582	168,663	345,745
Total	728,061	1,028,309	2,523,879

After calculating the DFT voltages and average EEFs, the DFTs were expressed as delivered energy using the following equation:

$$U = \frac{1}{2} CV^2 \quad \textbf{(2)}$$

Where U is the energy stored in the pulse generator of an implantable device, C is the capacitance of the pulse generator, assumed to be 140 μF, and V is the DFT in voltage. The average EEFs were squared, because the DFT energy is related to voltage squared. The data were normalized using min-max normalization to scale the data between zero and one, and a linear regression analysis was performed comparing the normalized DFT energies with the normalized average squared EEF voltages.

Results

Results from the finite element simulations are presented below, including plots of the electric field in the atrial myocardium and esophagus, DFT and EEF data, the results of the linear regression analysis and the mesh convergence data.

Mesh Convergence Study

The DFTs and total volumes of the atrial myocardium in the mesh convergence study are listed in Table 4. There was a 0.34% increase in the DFT comparing the coarse heart mesh to the fine heart mesh. Likewise, there was a 0.25% increase between the fine heart mesh and the finer heart mesh. As a result of this low percent increase the fine mesh was chosen for the ten simulations. Qualitative comparison of the electric field distribution in the atrial myocardium for each mesh indicate that the spatial distribution of electric field is not different between meshes (Figure 7).

Table 4: DFTs and Volumes of Atrial Myocardium in Mesh Convergence Study

Mesh Type	DFT (V)	Volume (mm^3)
Coarse	28.381	131,500
Fine	28.477	138,500
Finer	28.548	148,000

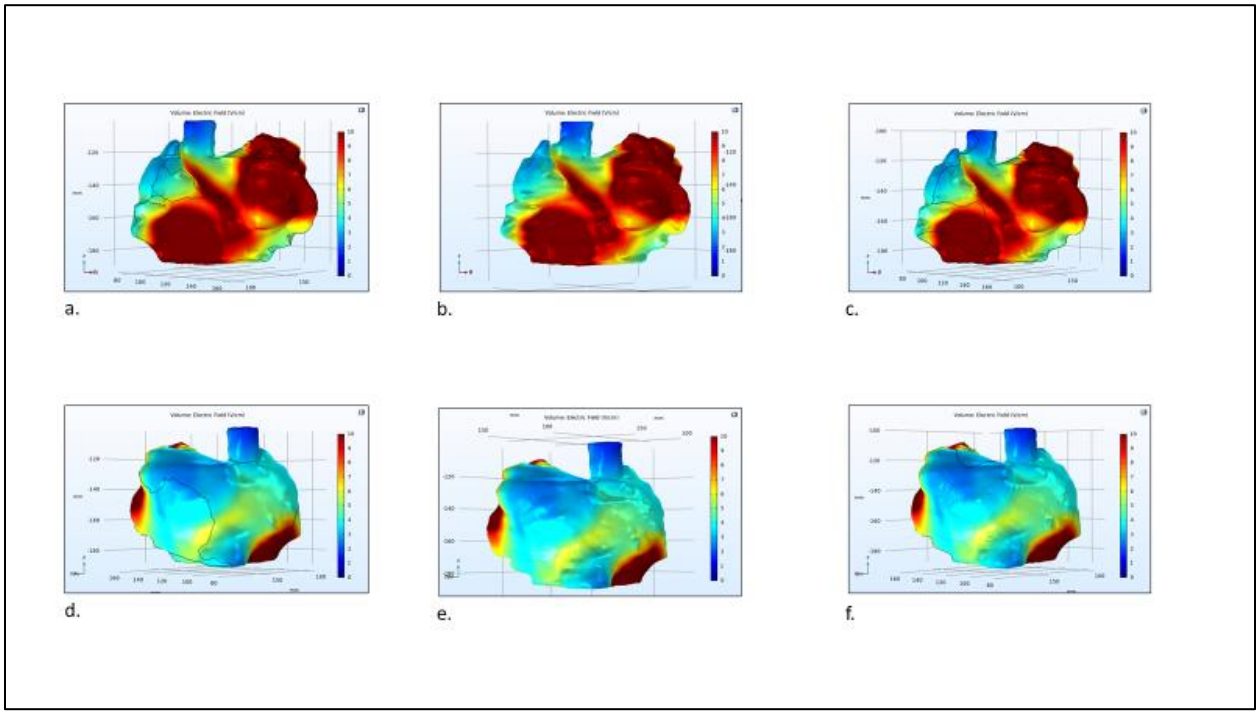

Figure 7: Anterolateral views of electric field in atrial myocardium of CS2_RAL1: a. coarse mesh; b. fine mesh; c. finer mesh, and posterolateral views of electric field in atrial myocardium of CS2_RAL1: d. coarse mesh; e. fine mesh; f. finer mesh of the mesh convergence study.

Electric Field Distribution

The following figures (Figures 8-12) show the electric field distribution in the atrial myocardium and the esophagus for four different electrode configurations with 200 V potential difference. The electric field distribution shifted throughout the right atrium in numerous electrode configurations based on the position of the right atrial electrode and produced varying DFTs and EEF values. The electric field remained fairly concentrated near the coronary sinus as the electrodes were shifted only slightly, whereas most of the variation was produced from the right atrial electrode due to the shifting of the electrode throughout the right atria. The electric field is heavily concentrated at the electrodes and disperses from them.

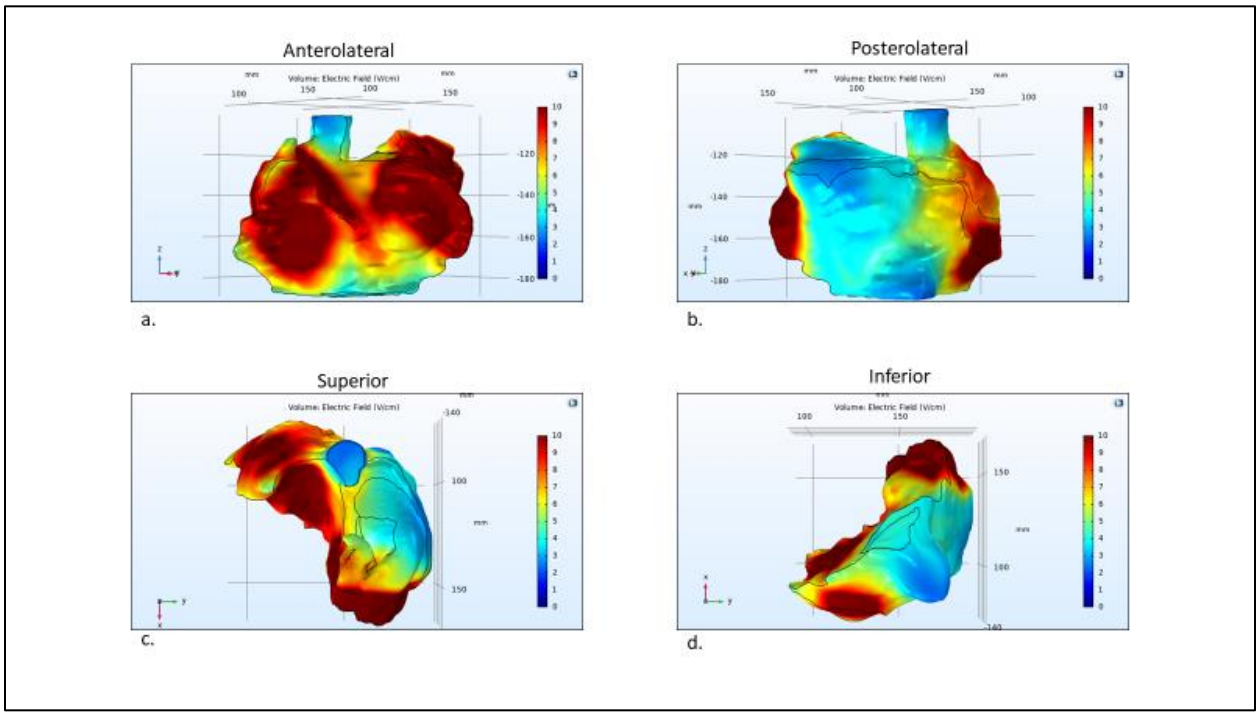

Figure 8: Electric field distribution in the atrial myocardium for CS1_RAL4 configuration in the atrial myocardium. A 200 V potential difference was applied between the electrodes. Electric field values are in V/cm.

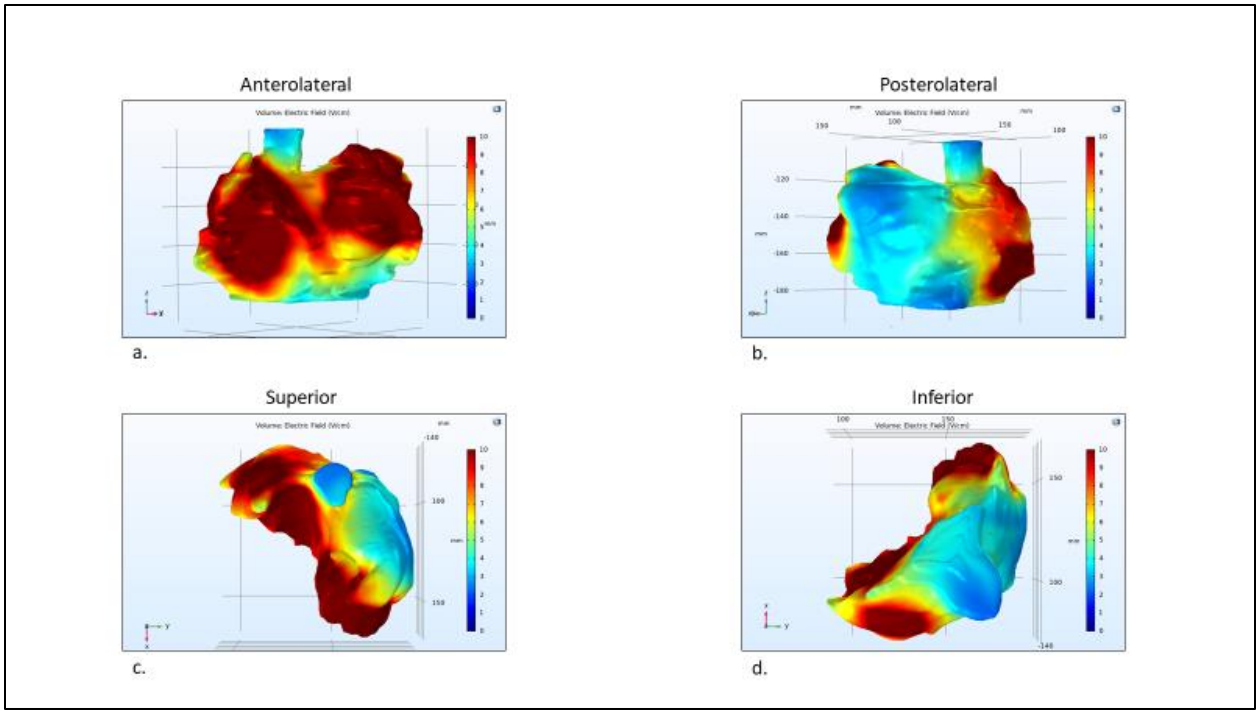

Figure 9: Electric field distribution in the atrial myocardium for CS2_RAL4 configuration in the atrial myocardium. A 200 V potential difference was applied between the electrodes. Electric field values are in V/cm.

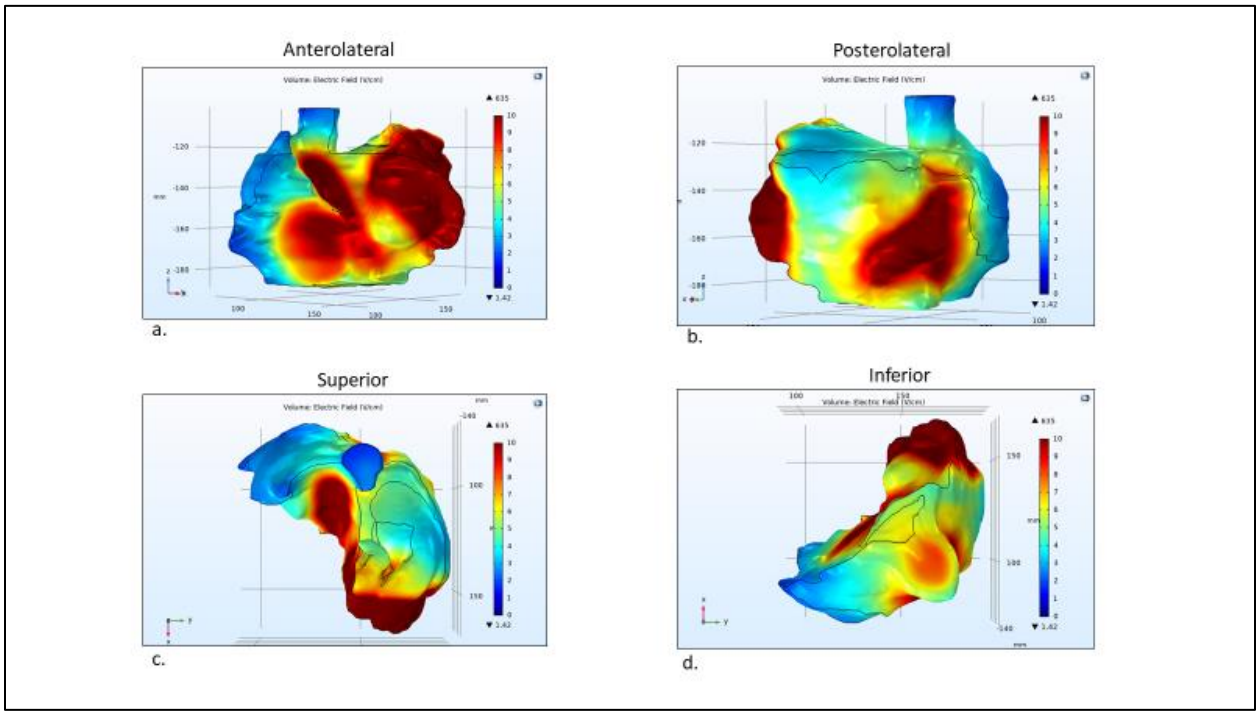

Figure 10: Electric field distribution in the atrial myocardium for CS1_RAS5 configuration in the atrial myocardium. A 200 V potential difference was applied between the electrodes. Electric field values are in V/cm.

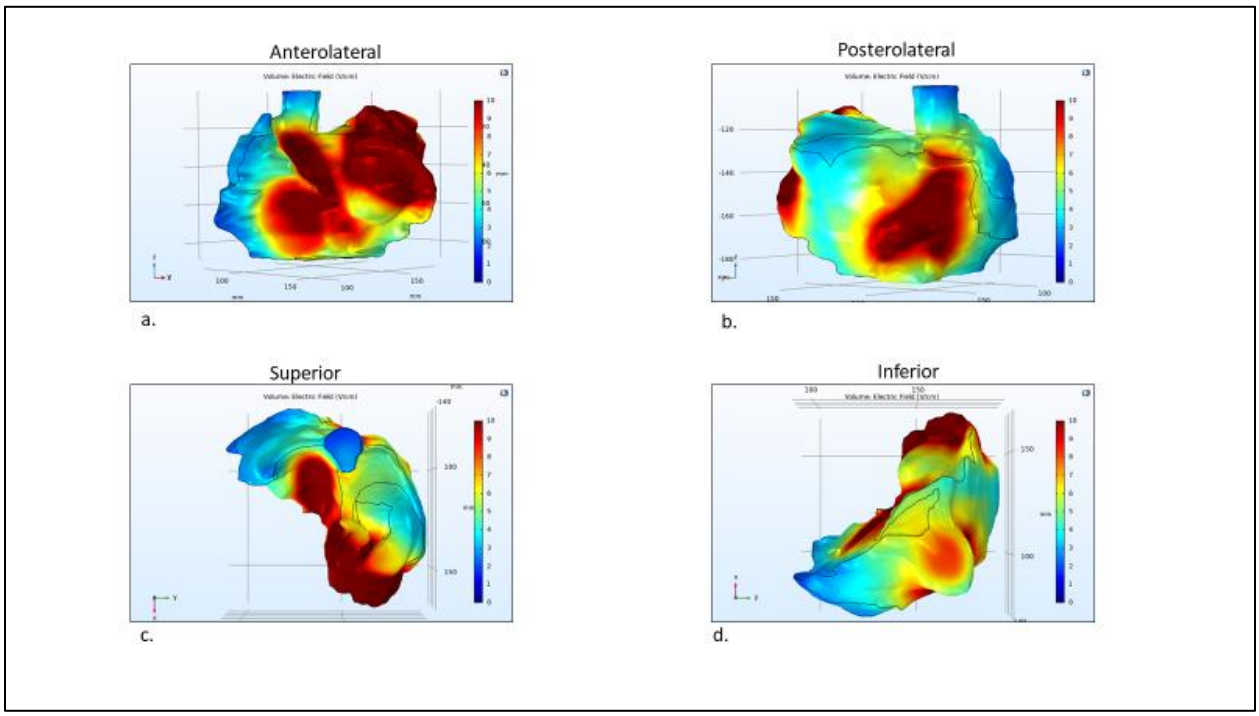

Figure 11: Electric field distribution in the atrial myocardium for CS2_RAS5 configuration in the atrial myocardium. A 200 V potential difference was applied between the electrodes. Electric field values are in V/cm.

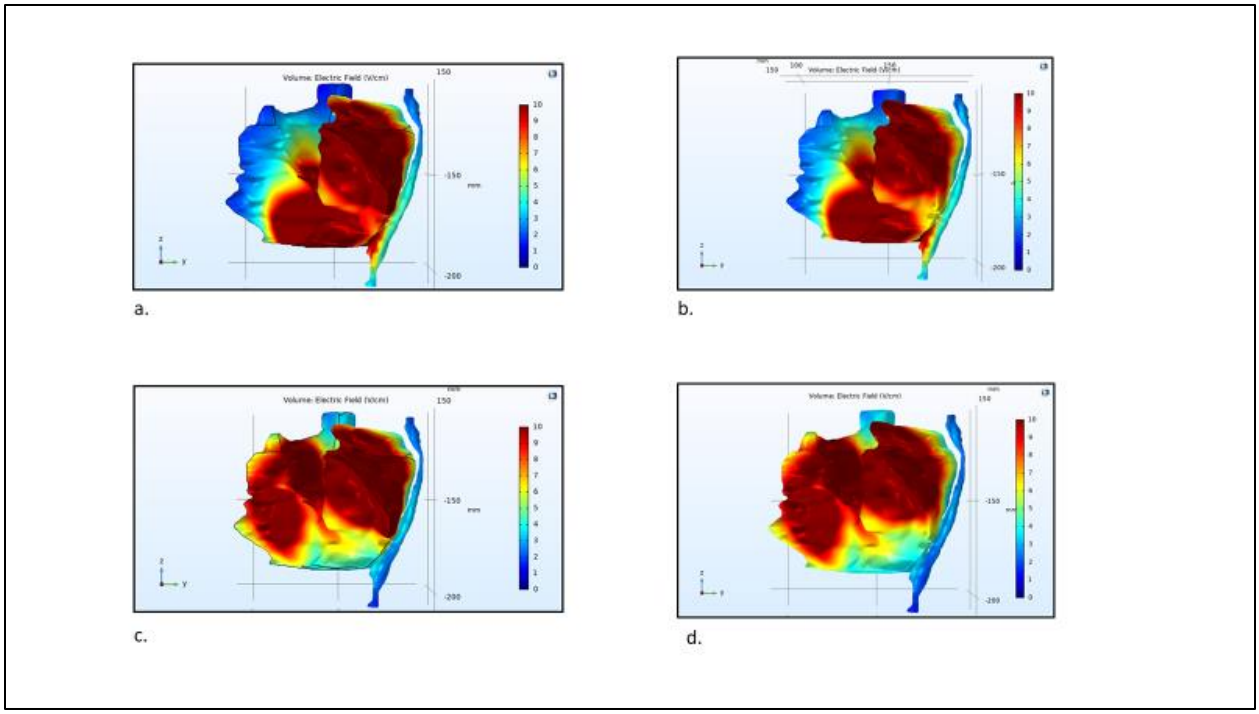

Figure 12:Lateral views of electric field distribution in the atrial myocardium and esophagus for four different electrode configurations: a. CS1_RAL3; b. CS2_RAL3; c. CS1_RAL4; d. CS2_RAL4; A 200 V potential difference was applied between the electrodes. Electric field values are in V/cm.

DFTs, Average EEFs, and Regression Analysis

The DFTs and average EEFs had similar values for both CS placements and shifting the right atrial electrode throughout the right atrium. Specifically, the CS electrode placement did not affect the average EEF or DFT for a given RA placement. For all ten configurations, there was a 42% increase in the DFT from the lowest to the highest DFT. Likewise, for the average EEF data, there was a 126% increase between the lowest and highest average EEFs. However, these EEF values did not correspond with the lowest and highest DFTs.

The non-normalized DFT data are given in Table 5 below. The average EEFs for each electrode configuration are shown below in Figure 13. A regression analysis compared the normalized DFTs with the normalized EEFs by calculating the coefficient of determination (R^2), shown in Figure 14 below. The data showed no relationship between the DFTs and average

EEFs, however there were several simulations with equal and low DFTs. RAL1 and RAS5 produced the lowest DFTs for both CS placements. It also appeared that a larger percent increase in the DFT occurred between the RAL electrodes in closer proximity to one another.

Table 5: DFT Voltages for Each Electrode Configuration

Electrode Configuration	DFT (V)	DFT (J)
CS1_RAL1	28	0.055
CS1_RAL2	34	0.08
CS1_RAL3	30	0.063
CS1_RAL4	33	0.076
CS1_RAS5	26	0.047
CS2_RAL1	28	0.055
CS2_RAL2	37	0.096
CS2_RAL3	31	0.067
CS2_RAL4	35	0.086
CS2_RAS5	28	0.055

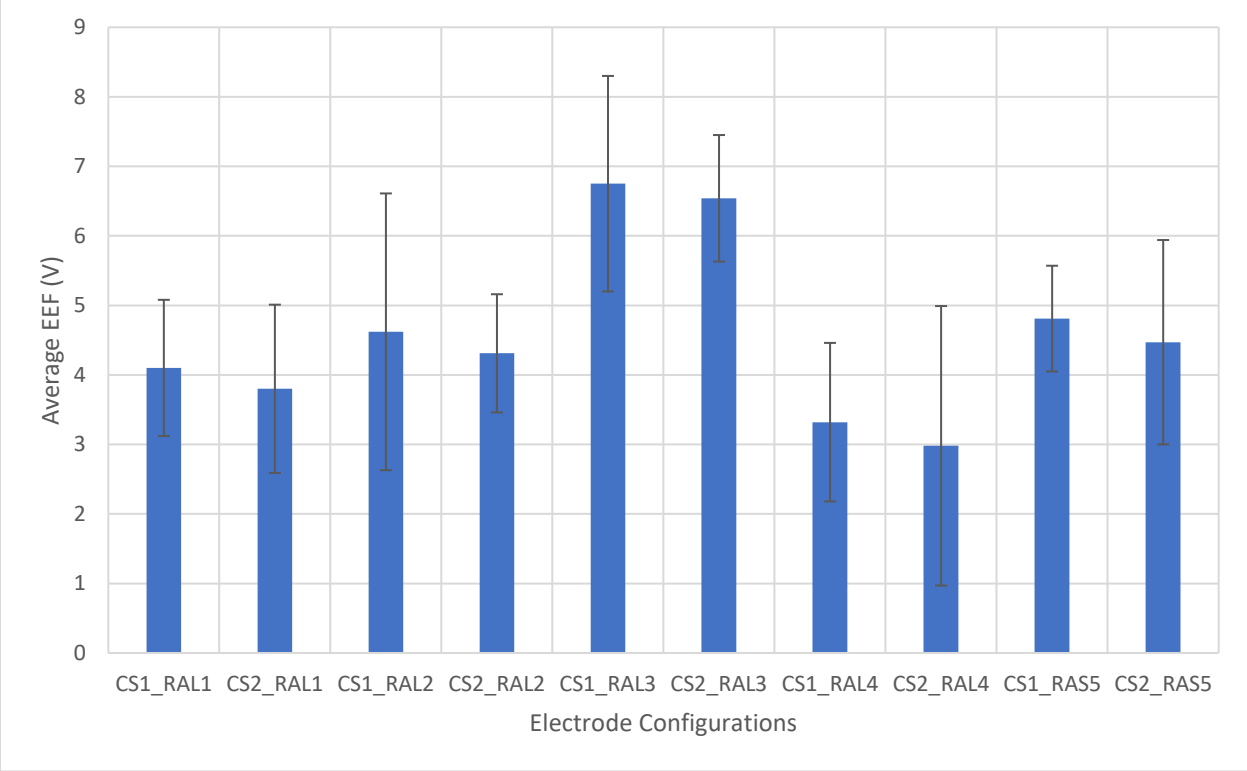

Figure 13: The average EEF with standard deviation bars for each electrode configuration. The average EEF was not influenced by the CS placement for a given RA placement.

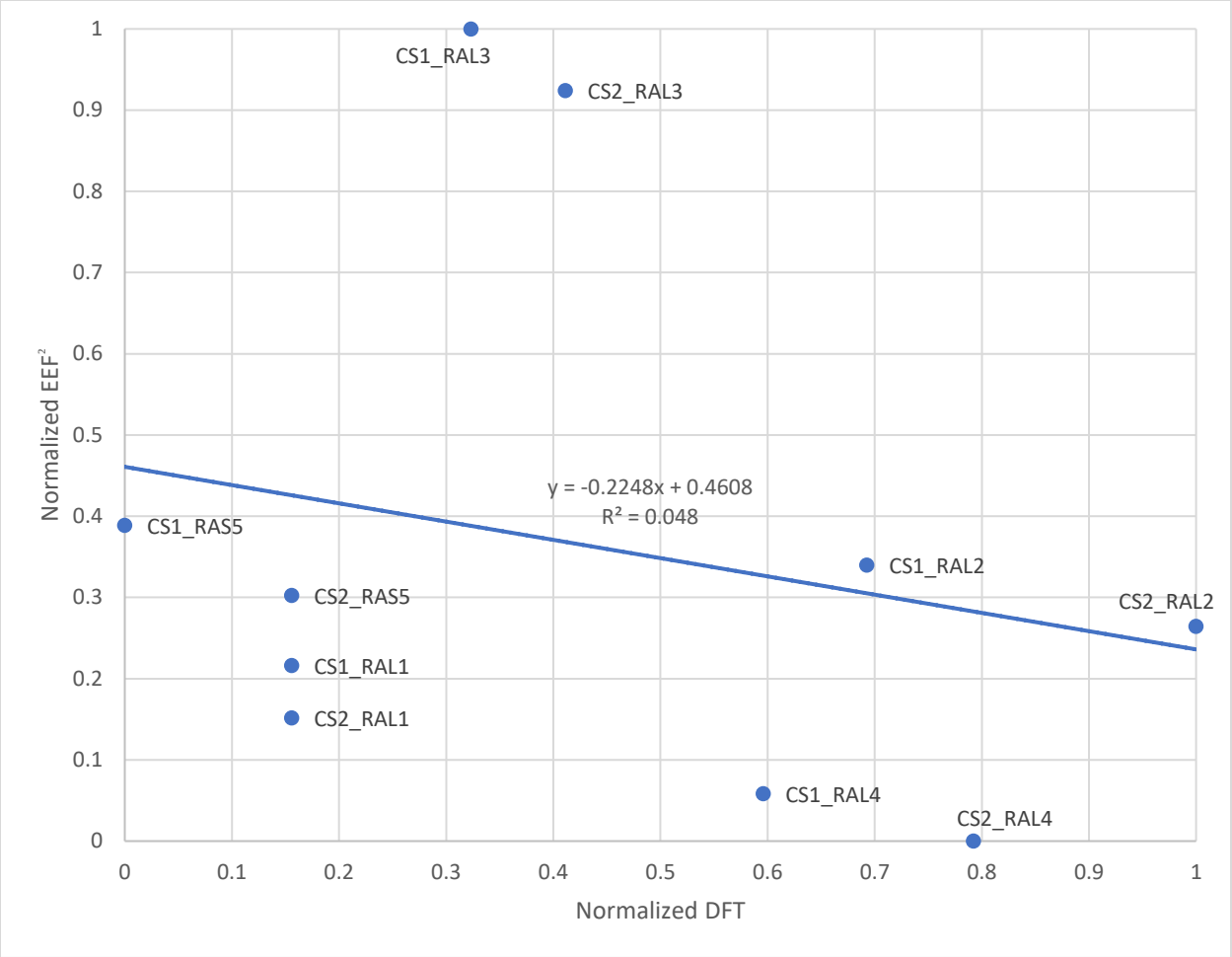

Figure 14: The comparison between the normalized DFTs and normalized average squared EEFs for each electrode configuration. The DFT energies and average squared EEF voltages were normalized. The coefficient of determination shows there is no relationship between the DFTs and average EEFs for these given electrode configurations.

Discussion

Previous studies on atrial DFTs and electrode placement have focused on external defibrillation or internal defibrillation studies in various animal models. For this work, internal defibrillation was investigated by developing a finite element analysis study conducted on an anatomically realistic, volume conductor model of the heart and surrounding organs of a human female. This study aided in determining variations in the DFT, average EEF adjacent to the left atrium and electric field distribution of the atrial myocardium by testing ten different clinically relevant internal electrode configurations.

Effect of Electrode Placement on DFTs and Average EEFs

This study simulated cardioversion shocks in an anatomically realistic model of the heart using finite element analysis and investigated the effect of various electrode placements on DFTs and average EEFs. However, a positive or negative relationship between the average EEFs and DFTs could not be determined. Despite this, several electrode configurations had low DFTs, with a 42% increase from the lowest to highest DFT. This data indicates that internal electrode placement is an important factor in lowering the delivered energy to the patient using an implantable defibrillator for treatment of AF. However, a relationship was not observed between the DFTs and the average EEFs, and the likelihood of predicting an optimal electrode placement based on the average EEF is still unknown. Perhaps the low sample size of ten electrode configurations was not sufficient. Testing more configurations could prove challenging, however, due to the limited space available in placing the coronary sinus electrode. Small shifts could be implemented along the right atrial lateral and septal walls to increase the number of electrode configurations. There is more room to spatially reconfigure the right atrial electrode, yet some reconfigurations would not be clinically viable. The average EEF may not be a predictor of the internal DFT, however various features of the average EEF could be utilized in a clinical setting. Previous studies have found a relationship between the average EEF and DFT for external cardioversion, suggesting that, in clinical practice, a physician could measure the EEF, shift the electrodes in small increments while continually measuring the EEF, and place the electrodes where the strongest EEF occurs, which would result in the lowest DFT.[21-22] If more internal configurations are tested and a similar relationship is discovered between the average EEF and DFT, perhaps a physician could perform a similar procedure. Additionally, another

intracardiac measure of electric field, such as in or near the interatrial septum or aortic chamber, could show a relationship between that measure and the DFT.

Model Limitations

The model developed for this study contained sufficient levels of resolution in the volume mesh to capture much of the cardiac detail needed to develop an anatomically realistic model for the purposes of this study. However, some of the vasculature was left out of the model, as it was challenging to segment, and including every detail and part of the geometry would lead to more tetrahedral elements further increasing the simulation times. Another limitation of this study was that the shock waveform was not specified. Even though Equation 2 is an adequate approximation for energy for a truncated exponential decay waveform in defibrillation devices, it could be useful to investigate the effects of different waveforms on the DFT. However, a different type of study would need to be conducted in COMSOL or a time varying feature would need to be implemented in the model for this study. Combining waveform optimization with this study could influence the DFT and average EEF. Also, a third limitation is that the model in this study was passive, meaning any effects of shock timing relative to activation distribution during AF was not modeled prior to delivering the shock. Nonetheless, the model is sufficient to study simulated cardioversion shocks and the effect of various electrode placements on the average EEF and DFT. Lastly, the limited number of electrode configurations could not determine a relationship between the DFTs and average EEFs.

Future Work

The goal of this study was to analyze the atrial DFTs and average EEFs adjacent to the left atrium in a volume conductor heart model with some surrounding organs by shifting the coronary sinus and right atrial electrodes. Testing more electrode configurations could give

insight into whether a relationship can be discovered between the atrial DFTs and the average EEFs. Also, changing the range of average EEF data that was analyzed could yield different results. Extracting EEFs from a more concentrated or expanded region of the esophagus could demonstrate a relationship between the DFT and EEF. It could possibly be useful to investigate any relationships between the EEF and DFT as a function of the spatial separation between and relative orientation of the coronary sinus electrode and the right atrial electrodes, as well as the impedance between the electrodes. It could also be beneficial to test different heart geometries from different patients and compare the DFTs and average EEFs between patients. Many times, cardiac treatments are patient-specific, and many factors can influence the type of treatment available and possible for a patient.

Conclusions

With the growing concerns of an increase in the prevalence of AF, investigating novel strategies to more effectively treat this arrhythmia with internal cardioversion and allow patients to live more normal, higher-quality lives is crucial to make breakthroughs in this field. Although a relationship could not be discovered between the average EEF and DFT, this study effectively simulated internal cardioversion shocks and has shown the effects of various electrode placements on the DFTs, resulting in low DFTs. Small shifts in the electrode placement can change the DFT by up to 42%, a significant change in the delivered energy, which could make the difference in a painful vs. nonpainful defibrillation threshold.

Regarding the relationship between the average EEF and DFT, future research could be devoted to testing more electrode configurations and a different region of the esophagus to determine whether a relationship exists for internal cardioversion. Also, a different intracardiac measure could be investigated as a predictor of the DFT. If a relationship can be discovered

between the EEF or another measure and the DFT, this relationship could aid a clinician in predicting patient-specific electrode placements in order to lower delivered energy to painless or tolerable levels.

References

1. Chugh, Sumeet S., et al. “Worldwide Epidemiology of Atrial Fibrillation.” *Circulation*, vol. 129, no. 8, 2014, pp. 837–847., doi:10.1161/circulationaha.113.005119.

2. Feinberg, William M. “Prevalence, Age Distribution, and Gender of Patients With Atrial Fibrillation.” *Archives of Internal Medicine*, vol. 155, no. 5, 1995, p. 469., doi:10.1001/archinte.1995.00430050045005.

3. Miyasaka, Yoko, et al. “Secular Trends in Incidence of Atrial Fibrillation in Olmsted County, Minnesota, 1980 to 2000, and Implications on the Projections for Future Prevalence.”

4. Krijthe, B. P., et al. “Projections on the Number of Individuals with Atrial Fibrillation in the European Union, from 2000 to 2060.” *European Heart Journal*, vol. 34, no. 35, 2013, pp. 2746–2751., doi:10.1093/eurheartj/eht280.

5. Schnabel, Renate B, et al. “50 Year Trends in Atrial Fibrillation Prevalence, Incidence, Risk Factors, and Mortality in the Framingham Heart Study: a Cohort Study.” *The Lancet*, vol. 386, no. 9989, 2015, pp. 154–162., doi:10.1016/s0140-6736(14)61774-8.

6. Go, Alan S., et al. “Prevalence of Diagnosed Atrial Fibrillation in Adults.” *Jama*, vol. 285, no. 18, 2001, p. 2370., doi:10.1001/jama.285.18.2370.

7. Kim, Michael H., et al. “Estimation of Total Incremental Health Care Costs in Patients With Atrial Fibrillation in the United States.” *Circulation: Cardiovascular Quality and Outcomes*, vol. 4, no. 3, 2011, pp. 313–320., doi:10.1161/circoutcomes.110.958165.

8. Nguyen, Tu N., et al. “Review of Epidemiology and Management of Atrial Fibrillation in Developing Countries.” *International Journal of Cardiology*, vol. 167, no. 6, 2013, pp. 2412–2420., doi:10.1016/j.ijcard.2013.01.184.

9. Wilber, DJ, Pappone C, Neuzil P, et al. Comparison of Antiarrhythmic Drug Therapy and Radiofrequency Catheter Ablation in Patients with Paroxysmal Atrial Fibrillation: A Randomized Control Trial. *JAMA.* 2010;303(4):333-340. doi:10.1001/jama.2009.2029

10. Haïssaguerre, Michel, et al. “Successful Catheter Ablation of Atrial Fibrillation.” *Journal of Cardiovascular Electrophysiology*, vol. 5, no. 12, 1994, pp. 1045–1052., doi:10.1111/j.1540-8167.1994.tb01146.x.

11. Cooper RAS, Alferness CA, Smith WA, et al. Internal cardioversion of atrial fibrillation in sheep. Circulation. 1993;87:1673–1686.

12. Alt E, Schmitt C, Ammer R, et al. Initial experience with intracardiac atrial defibrillation in patients with chronic atrial fibrillation. PACE. 1994;17:1067–1078

13. Kalman, Jonathan M., et al. “Low Energy Endocardial Cardioversion of Atrial Arrhythmias in Humans.” *Pacing and Clinical Electrophysiology*, vol. 18, no. 10, 1995, pp. 1869–1875., doi:10.1111/j.1540-8159.1995.tb03834.x.

14. Lévy, Samuel, and Philippe Richard. “Is There Any Indication for an Intracardiac Defibrillator for the Treatment of Atrial Fibrillation?” *Journal of Cardiovascular Electrophysiology*, vol. 5, no. 11, 1994, pp. 982–985., doi:10.1111/j.1540-8167.1994.tb01137.x.

15. Saksena, Sanjeev, et al. “Clinical Efficacy and Safety of Atrial Defibrillation Using Biphasic Shocks and Current Nonthoracotomy Endocardial Lead Configurations.” *The American Journal of Cardiology*, vol. 76, no. 12, 1995, pp. 913–921., doi:10.1016/s0002-9149(99)80261-6.

16. Boriani, Giuseppe, et al. “Mechanisms of Pain Associated with Internal Defibrillation Shocks: Results of a Randomized Study of Shock Waveform.” *Heart Rhythm*, vol. 2, no. 7, 2005, pp. 708–713., doi:10.1016/j.hrthm.2005.03.024.

17. Gerstenfeld, Edward P., and Thomas H. Everett. “Internal Atrial Defibrillation Revisited: How Low Can We Go?” *Journal of the American College of Cardiology*, vol. 63, no. 1, 2014, pp. 49–51., doi:10.1016/j.jacc.2013.06.066.

18. Manoharan, Ganesh, et al. “Comparing the Efficacy and Safety of a Novel Monophasic Waveform Delivered by the Passive Implantable Atrial Defibrillator With Biphasic Waveforms in Cardioversion of Atrial Fibrillation.” *Circulation*, vol. 109, no. 13, 2004, pp. 1686–1692., doi:10.1161/01.cir.0000124068.69162.4e.

19. Mitchell, A. “What Is the Optimal Electrode Configuration for Atrial Defibrillators in Man?” *Europace*, vol. 4, no. 1, 2002, pp. 41–44., doi:10.1053/eupc.2001.0207.

20. Yang, Fei, et al. “A Novel Electrode Placement Strategy for Low-Energy Internal Cardioversion of Atrial Fibrillation: A Simulation Study.” *International Journal of Cardiology*, vol. 158, no. 1, 2012, pp. 149–152., doi:10.1016/j.ijcard.2012.04.027.

21. Fitch DA, de Jongh Curry AL. Esophageal electric fields are predictive of atrial cardioversion success—a finite element analysis. Ann Transl Med 2015;3(14):196. doi: 10.3978/j.issn.2305-5839.2015.08.17

22. Fitch, David A., et. al. “Esophageal Electric Fields Are Predictive of Atrial Defibrillation Thresholds.” *Pacing and Clinical Electrophysiology*, vol. 35, no. 3, 2011, pp. 335-340., doi:10.1111/j.1540-8159.2011.03291.x

23. “HeartPrint® Imaging Guidelines.” *Materialise*, Aug. 2016, www.materialise.com/system/files/uploads/resources/Scan%20protocols/l10099_heartprint_imaging_protocol.pdf.

24. Depré Christophe, et al. *Atlas of Cardiac MR Imaging: with Anatomical Relationships*. Kluwer Academic Publishers, 1991.

25. "3D Printing Software and Services." *Materialise*, www.materialise.com/en

26. Rush, Stanley, et al. "Resistivity of Body Tissues at Low Frequencies." *Circulation Research*, vol. 12, no. 1, 1963, pp. 40–50., doi:10.1161/01.res.12.1.40.

27. Geddes, L. A., and L. E. Baker. "The Specific Resistance of Biological Material—A Compendium of Data for the Biomedical Engineer and Physiologist." *Medical & Biological Engineering*, vol. 5, no. 3, 1967, pp. 271–293., doi:10.1007/bf02474537.